Article

Viral plasticity facilitates host diversity in challenging environments

Juan A. Bonachela [1] ✉

The antagonistic coevolution of microbes and viruses influences fundamentally the diversity of microbial communities. Information on how environmental variables interact with emergent defense-counterdefense strategies and community composition is, however, still scarce. Following biological intuition, diversity should increase with improved growth conditions, which offset evolutionary costs; however, laboratory and regional data suggest that microbial diversity decreases in nutrient-rich conditions. Moreover, global oceanic data show that microbial and viral diversity decline for high latitudes, although the underlying mechanisms are unknown. This article addresses these gaps by introducing an eco-evolutionary model for bacteria-virus antagonistic coevolution. The theory presented here harmonizes the observations above and identifies negative density dependence and viral plasticity (dependence of virus performance on host physiological state) as key drivers: environmental conditions selecting for slow host growth also limit viral performance, facilitating the survival of a diverse host community; host diversity, in turn, enables viral portfolio effects and bet-hedging strategies that sustain viral diversity. From marine microbes to phage therapy against antibiotic-resistant bacteria or cancer cells, the ubiquity of antagonistic coevolution highlights the need to consider eco-evolutionary interactions across a gradient of growth conditions.

Unraveling the role that viruses play in the dynamics and composition of microbial communities is a fundamental question especially important in the case of marine ecosystems, where viruses are massively abundant[1–3]. By killing their host cell, lytic viruses disrupt the flow of energy and nutrients to higher trophic levels of the marine food web. Moreover, the cellular contents resulting from lysis fuel the marine microbial loop, main responsible for oceanic primary production. Further, viral mortality, together with biotic factors such as grazers and abiotic factors such as nutrient availability and temperature, determine the biogeography of marine microbes[1,4]. Thus, the influence of marine viruses ripples across spatial, temporal, and organizational scales, affecting local and global biogeochemistry and ecosystem services[5].

Central to the understanding of how marine viruses shape microbial communities is unveiling which mechanisms drive the antagonistic coevolution of hosts and viruses across gradients of environmental conditions[6]. Among other evolutionary strategies, hosts can achieve resistance through modification of parts of the host genome (the clustered regularly interspaced short palindromic repeats/CRISPR-associated sequences system), or by modifying the receptors that the virus uses as a gateway to infection (adsorption inhibition)[7,8]. As an example of the latter, the bacterium *Escherichia coli* can modify receptors such as lipopolysaccharide (LPS) or produce proteins to mask outer-membrane protein A (OmpA), used by T viruses to adsorb to the cell surface. In turn, viruses can evolve counter-defense mechanisms, for example modifying their tail fiber to recognize and attach to altered forms of the receptor or new receptors altogether, thus increasing its host range[7–9] (see Fig. 1a). Although evolutionary costs are key to these coevolutionary dynamics[6], how costs and associated tradeoffs are influenced by environmental

[1]Department of Ecology, Evolution, and Natural Resources, Rutgers University, New Brunswick 08901, USA. ✉e-mail: juan.bonachela@rutgers.edu
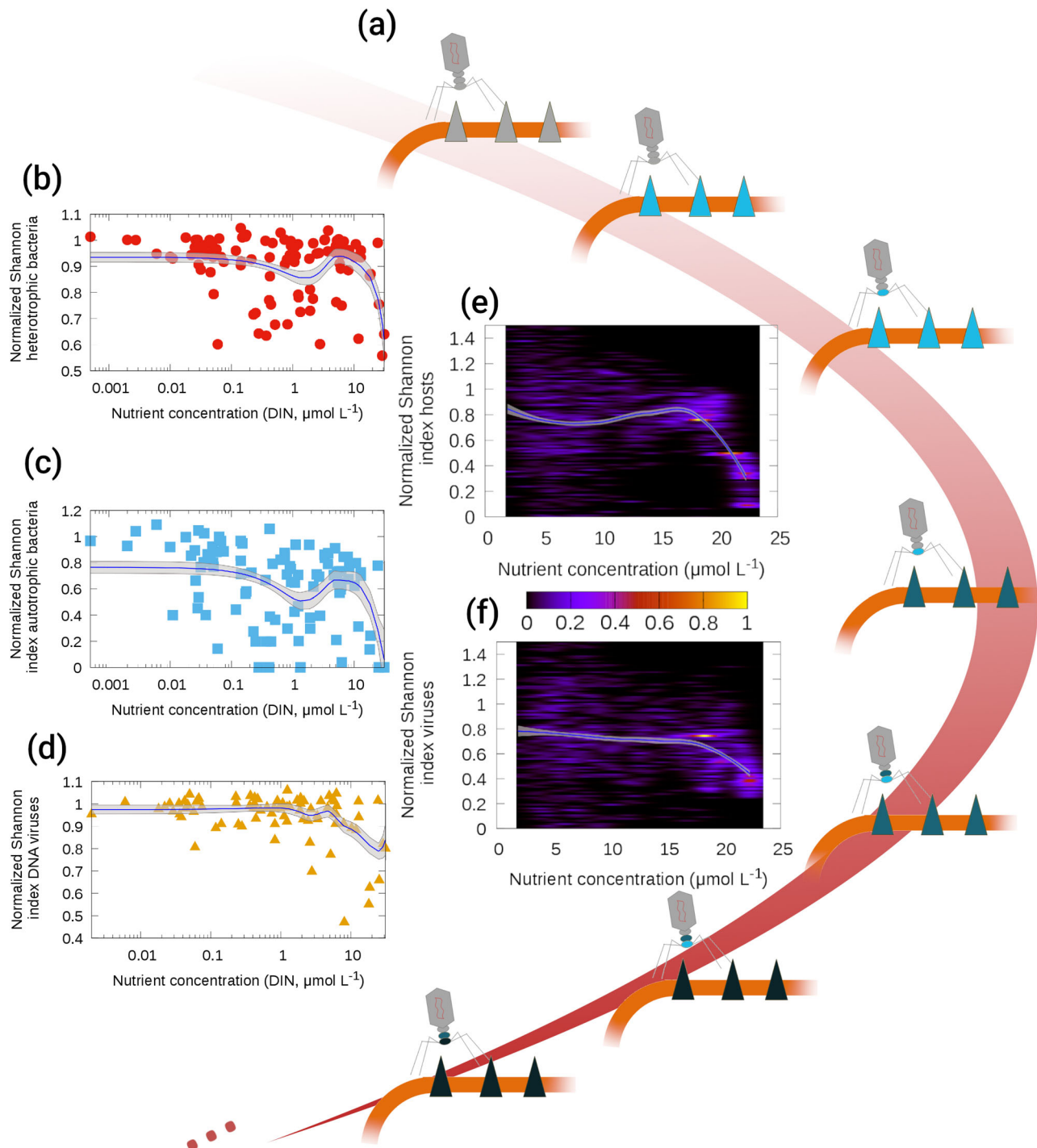
Fig. 1 | Coevolution and diversity. a Illustration of a few steps of the coevolution of host and virus modeled here (red arrow represents time), starting from a pristine form of the receptor and tail fiber (gray color): for the host, the darker the blue shade of the receptor the more it departs from the pristine form, i.e. more host innovation and thus higher tax on the cell's maximum growth rate; for the virus, the more shades of blue the tail shows (here indicated in the sheath for visualization) the more receptor forms can be recognized, i.e. more versatile virus and thus higher tax on tail fiber efficacy. These steps are influenced by viral plasticity (dependence of viral infection time and offspring number on host growth rate, Fig. S1d–e). **b**–**d** Biodiversity as a function of environmental nutrient measured by the Tara Oceans expedition across the globe (**b**, **c**, heterotrophic and phototrophic bacteria, 106 dots and 104 squares, respectively[31]; **d**, DNA viruses, 86 triangles[32]); nutrient refers to total nitrate and nitrite, for simplicity referred to here as dissolved inorganic nitrogen (DIN), see SI.7 for further details. **e**, **f** Biodiversity as a function of environmental nutrient measured in our simulations (1059 points, with colors representing occurrence probability); a version of the model that neglects viral plasticity did not show any discernible pattern (Fig. S14). In all panels, lines and shaded area represent a LOESS smoothing and corresponding confidence interval, respectively, for visual indication of trend and variability only: host diversity is approximately constant for mid to low nutrient, but declines steeply for high nutrient availability; the pattern is similar but less pronounced for viruses. All panels show high variability in biodiversity for mid-nutrient levels, leading to the "fluctuating" index around a saturating value. We normalized data by that apparent saturation value to facilitate comparison across cases. LOESS lines obtained using the R functions *loess* and *predict* with default options.

conditions is poorly understood and understudied. Common biological intuition dictates that adverse environments deter coevolution due to increased direct costs and reduced indirect benefits of evolving resistance[10–12]. However, the limited available experimental work investigating antagonistic coevolution under contrasting growth environments[10,11,13] that also studied diversity has instead reported higher host diversification when growth conditions decline[13]. It is also unclear under which environmental conditions the coevolutionary process results from continuous innovation (i.e. arms races), an alternation of strategies that are revisited (fluctuating selection/Red-Queen dynamics), or a combination of the two[11,14–17].

In addition, empirical work studying coevolution has traditionally overlooked that host physiological state inherently constrains the ecological and evolutionary response of the virus. Because, due to its parasitic nature, the virus relies on host resources and machinery for reproduction, key viral life-history traits such as infection time (latent period) and offspring number (burst size) change with the host's physiological state[18–25], dependence that has been termed viral plasticity. Specifically, an improved host physiological state typically leads to shorter but more productive infections (smaller latent periods and larger burst sizes, see e.g.[18,20,22] or Fig. S1d-e). However, empirical work devoted to understanding the links between host growth conditions and viral reproduction[19,20,22–30] focuses on short timescales (one infection cycle), and thus whether or how viral plasticity influences antagonistic coevolution is still unknown.

The dearth of such important pieces of the coevolutionary puzzle hinders our understanding of how viral pressure, influenced by bottom-up sources of regulation such as resource availability, dynamically shapes the microbial community in the oceans in the short and the long term. For example, the Tara Oceans expedition recently reported diversity latitudinal patterns that are similar for microbial hosts and viruses[31,32]; leveraging these data, we represented here diversity against the reported nutrient gradient (as a proxy for host growth conditions), which unveiled a pattern seemingly conserved across eukaryotes, bacteria, and the DNA viruses that infect them (Fig. 1b–d and Fig. S15a–d): biodiversity is high for challenging growth conditions (low nutrient), remains constant as conditions improve, and decreases steeply for favorable growth conditions (high nutrient). The ecological and/or evolutionary mechanisms that underlie this and the original latitudinal pattern are, however, unknown.

The knowledge gaps above also handicap models built to understand and predict host-virus dynamics and emergent consequences such as diversity, primary production, or carbon export, key to assessing the future of our oceans under any global climate change scenario. Here, we contribute to bridging these gaps by introducing a theoretical model for host-virus antagonistic coevolution that accounts for viral plasticity. We find that the changeable viral performance associated with viral plasticity can reduce evolutionary costs for the host and facilitate survival, as well as a variety of evolutionary strategies, under growth-limiting conditions. For all environments in our simulations, coevolutionary dynamics initially lead to arms races but ultimately converge to fluctuating selection. Host and virus behavior and diversity emerging from such coevolutionary dynamics, shaped by negative density dependence within and across phenotypes, resemble empirical observations.

Results and discussion
Model for the coevolution of a microbial host and a plastic virus
Our model focuses on host changes in receptors and viral changes in tail fiber, which have been documented to arise quickly and generically across host-virus systems in a variety of contexts[6–8,14,15,33,34]. These evolutionary strategies entail important tradeoffs. For example, modifying the receptor may lead to reduced functional efficacy (e.g. reduced uptake affinity or uptake rate), and changes in the tail fiber may lead to reduced efficiency attaching to the receptors that it can

recognize[6,8,14,35–37]. Indirect costs include antagonistic pleiotropy, as a receptor change that eludes a viral strain may make the host susceptible to another viral strain[38,39]. In our model, the initial host phenotype population is characterized by a pristine form of a focal receptor that is targeted by an initial virus phenotype population (Fig. 1a). As host and virus interact, random mutations lead to new host phenotypes that express only a phenotype-specific modified form of the receptor. This modification decreases uptake and, ultimately, the maximum growth rate of the new host phenotype proportionally to its degree of innovation (i.e. to how much the receptor departs from its pristine form, Fig. S1b). In turn, random mutations in the virus tail fiber introduce new virus phenotypes that target different forms of the receptor; these new viral phenotypes, however, show a reduction of adsorption rate proportional to their degree of versatility (i.e. to how many forms of the receptor the tail fiber can recognize, Fig. S1c). We parametrized the model to E. coli hosts and T7 viruses, but the framework can be tailored to other examples. Our model also incorporates dependencies between the value of the main viral traits and host growth rate (as a proxy for host physiological state)[40] that have been quantified experimentally for this system[20,22,24,25]. Moreover, because rapid evolution alters the latent period within hours[41], here we utilized a theoretical prescription for the (plastic) optimal value of the latent period, expression that is valid for different environments[40,42].

We used a chemostat as environmental context, adjusting the input nutrient concentration and dilution rate to generate a variety of relevant growth conditions here characterized by the nutrient available within the chemostat (realized nutrient, Fig. S4a). Shaped by biotic and abiotic factors, realized nutrient is an environmental variable routinely measured in empirical work, which enables comparison of our results with existing observations. In marine ecosystems, oligotrophic conditions are expected in e.g. warm tropical waters, and eutrophic conditions in colder or coastal waters or upwelling events. Following Liebig's law of the minimum we assumed limitation by one single nutrient, but the framework can be straightforwardly generalized to multiple growth-limiting factors. See details about our framework, modifications, assumptions, and existing antagonistic coevolution models in Methods.

With such a setup, multiple host phenotype populations dynamically competed for the available nutrient, and (plastic) virus phenotypes competed for common hosts, ultimately reaching their asymptotic eco-evolutionary dynamics after an initial transitory period (Fig. S3a–h).

Viral plasticity facilitates host survival and diversification when growth conditions deteriorate
As simulated environments deteriorated (lower realized nutrient, resulting from lower dilution, Fig. S4a) more host phenotypes coexisted, characterized by receptors that departed further from the pristine form (Figs. 2a and S13a). This increase occurred despite the associated evolutionary cost and the lower resource level, both of which contribute to lowering growth rates (Fig. S1b, Methods, and Eq. (5)); for such dilution rates, a version of the model that neglects plasticity produced the collapse of the community (see Methods).

The increasing survival of host phenotypes (i.e. higher host richness) and increasing degree of innovation despite the lower growth rates that are selected for seem paradoxical (e.g.[11]), but can be understood in light of viral plasticity. The decrease in host growth rate associated with a lower nutrient availability affected viral productivity (reduced offspring and increased infection time, Fig. S1d-e). The reduced viral performance alleviated pressure on the host, which we hypothesize made affordable the evolutionary cost of modifying the receptor. Innovating, in turn, decreased the maximum growth rate of the mutant host, therefore decreasing further the performance of infecting viruses and facilitating the survival of the innovating host phenotype. The fact that the nonplastic version of the model collapsed for low dilutions excludes the reduced dilution-related background
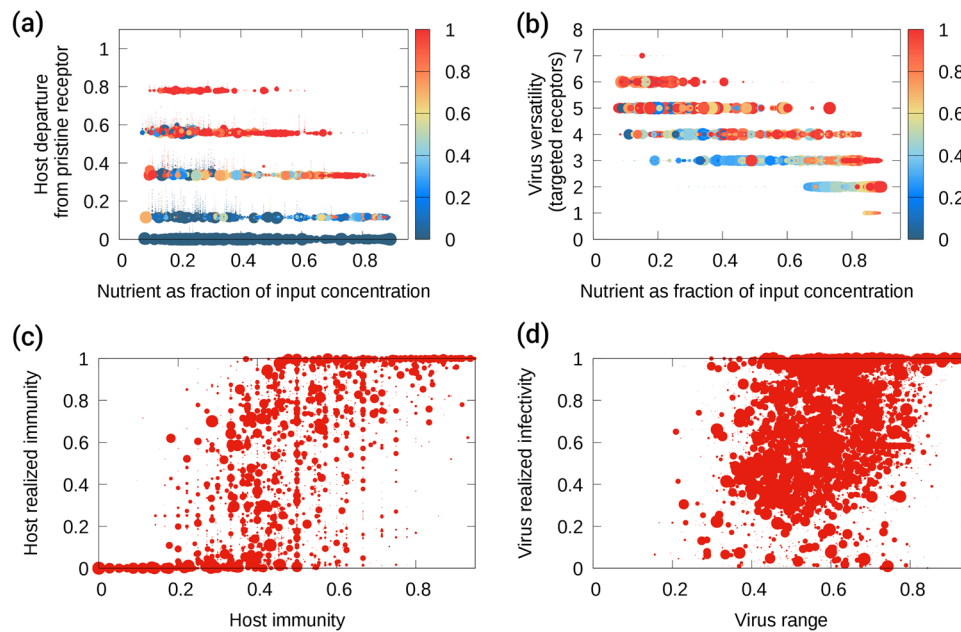
Fig. 2 | Coevolutionary strategies and consequences. a Host degree of innovation as a function of realized nutrient availability, with color representing the associated realized immunity (proportion of total viral abundance excluded by the host). **b** Viral versatility as a function of nutrient availability, with color representing the associated realized infectivity (proportion of total host abundance targeted by the virus). **c** Threshold-like relationship between proportion of phenotypes avoided by a host and its realized immunity; a classic host immunity ≥ 25% was needed for the phenotype to achieve a significant realized immunity, and ≥ 90% practically guaranteed that the host was an effective escape variant. **d** Threshold-like relationship between proportion of phenotypes targeted by a virus (range) and its realized infectivity; only ranges ≥ 30% produced significant infectivity, with range ≥ 85% practically ensuring total generalism. In all panels, point size represents the phenotype's relative abundance; data correspond to snapshots at $t = 10^5 d$ for the reference input concentration, across 100 replicates of our eco-evolutionary simulations to ensure a thorough sampling of the behavior of the system. See SI for details.

mortality as responsible for the increased richness and survival. Thus, viral plasticity generated a feedback loop that effectively reduced evolutionary costs and increased evolutionary benefits for the host, altering the competitive ability of host strategies predicted by standard models (which neglect viral plasticity), and therefore the expected host community structure (see Supplementary Information sections SI.2–SI.7).

Viral portfolio effects and bet-hedging emerge when host growth declines

Although abundance and therefore the kill-the-winner mechanism[43] was also at play, viral phenotypes did not necessarily target the most abundant hosts. While such a negative density dependence inescapably occurred (as it is a built-in component of the host-virus dynamics, see Methods and SI.7), viral plasticity made host quality also a relevant factor. Thus, as environments deteriorated we observed more virus phenotypes and, despite the consequent reduction in adsorption efficiency, an increased virus versatility (Fig. 2b, S1c, and S13b).

Differently from classic expectations, this viral diversification did not necessarily result from the need of the virus to track the increasingly different receptor, since a pool of hosts with the pristine receptor remained in many replicates (Fig. 2a). Increasing tail-fiber versatility, however, seemingly reduced viral niche overlap and therefore competition, progressively important as viral performance (indirectly) decreased with nutrient. Since the simulated viral community originated from a single initial phenotype, increasing versatility allowed new phenotypes to differentiate themselves from the common ancestor and each other (see Methods and SI). Nonetheless, in simulated or real communities of unrelated phenotypes, increasing versatility should typically lead to increased niche overlap. Whether to keep up with host evolution or to reduce competition, viral mutants here targeted a wider range of hosts as conditions became more challenging (portfolio effect), with most viruses retaining the ability to infect

the pristine form of the receptor thus bet-hedging the risks of their evolutionary investment in versatility (Fig. S7a).

Constrained evolutionary strategies in improved environmental conditions

Environments resulting in high nutrient concentrations (typically due to high dilution rates) led to reduced host and virus diversification (Fig. 2a, b). Favorable host growth conditions enabled a high viral performance (Figs. S1d-e), which a priori would justify host evolution. However, the combination of high nutrient, frequent dilution, viral pressure, and the evolutionary cost of evolving trivially selected for opportunistic strategies. Hosts prioritized resource uptake and fast growth over defense, which led to many coexisting phenotypes with receptors similar to the pristine form. In turn, low versatility was a cost-effective strategy allowing viruses to focus on the abundant pool of hosts with pristine receptors, which translated into a lack of evolutionary incentives also for the virus.

Past experiments with chemostats that achieved contrasting host growth conditions has reported higher strategy diversification for low than for high nutrient concentrations[13]. Our results suggest that the feedback between host physiological state, viral plasticity, and coevolutionary responses as the environment (and thus costs) change is responsible for this observation. Coevolutionary experiments able to resolve more systematically nutrient gradients, however, are needed to confirm empirically our hypothesis.

Classic immunity and range do not necessarily lead to realized immunity or infectivity

As expected, the fraction of existing virus phenotypes excluded by a focal host increased with the degree of host innovation (Fig. S7b). This "classic immunity", however, did not necessarily materialize in a higher proportion of excluded viral abundance (realized immunity, Fig. 2c), as only excluding a high-enough proportion of viral phenotypes ensured

the avoidance of the dominant phenotypes. Indeed, colors in Fig. 2a show that only hosts that invested sufficiently in departing from the pristine form of the receptor were rewarded with the highest realized immunity for a given realized nutrient concentration and replicate, which enabled their survival despite the associated evolutionary cost. Such a strategy, however, did not necessarily translate into a high relative abundance for the phenotype (dot size in same figure), which in turn limited the degree of innovation. The latter evidences the tradeoff between evolving towards more effective resource competition strategies and more effective defense strategies.

Similarly, the range of the virus (proportion of host phenotypes that a focal virus can infect) increased with the versatility of the phenotype's tail fiber (Fig. S7c), which did not necessarily lead to a higher realized infectivity (proportion of host biomass infected by the virus, Fig. 2d). Nonetheless, sufficiently versatile viral phenotypes achieved the highest realized infectivity for a given nutrient concentration and replicate, justifying the evolutionary investment (Fig. 2b).

Richness and biodiversity decrease when growth conditions improve

The increase in richness observed for both host and virus as environmental conditions declined (Figs. S13a and S13b) did not lead to communities with higher biodiversity (Shannon index[44], which accounts for the relative abundance of each phenotype, see Methods and Fig. 1e and f). Instead, biodiversity showed a seemingly constant behavior that decreased abruptly only in correlation with high nutrient concentrations. A similar pattern resulted when relaxing some of the assumptions of the model (e.g. letting latent period evolve as well, instead of imposing optimality), and was partially or totally lost when ignoring plasticity and for high input concentrations (see SI.7 and SI.9 for details).

Systematic measurements of microbial and viral diversity along environmental gradients are scarce. At a regional level, an increase of bacterial richness with a decreasing nutrient availability has been reported[45], thus qualitatively agreeing with our predictions (Fig. S13a). At the global level, the biodiversity patterns we obtained with the Tara Oceans data for bacteria, protists, and DNA viruses also resembled our predictions (Fig. 1b–d and Fig. S15a–d). The biodiversity pattern disappeared, however, when considering RNA viruses or data from all depths (Fig. S15e).

Despite the limitations of our model (see below and SI.9), the qualitative similarity between our results and the empirical observations above supports the idea of antagonistic coevolution as an important driver for bacterial and viral diversity in the oceans. These antagonistic coevolutionary responses emerging under the oceanic gradients of growth-limiting factors (e.g. temperature or various nutrients) would be mediated by viral plasticity, which links bottom-up and top-down sources of regulation and thus links two community-shaping mechanisms typically studied separately. In our simulations, negative density dependence between host and virus (i.e. killing the winner mechanism[43]) and among phenotypes equalized the host community as expected, leading to a variety of similarly abundant phenotypes regardless of environmental conditions (see SI.9.4). For adverse host growth conditions (here represented by low realized nutrient), viral plasticity facilitated the survival of host strategies otherwise not competitive. The latter led to a background of low-abundance phenotypes, which explains the increase in host richness but constant biodiversity. Occasionally, the stochasticity of the dynamics between coevolving hosts and viruses and with the environment may have led to the unexpected rise of one such background phenotypes to overwhelming dominance, which explains the noise around the main biodiversity pattern. In the model, these spurious events more rarely occur under higher overall competition imposed by increasing environmental drivers or (moderately) higher negative density dependence (see SI.8 and SI.9.2).

Host diversity and abundance enabled viral diversity but did not determine it as, through viral plasticity, host quality also influenced the success of a viral strategy. As a result, viral biodiversity resulted in a similarly constant but noisier pattern despite the steep increase of richness observed as growth conditions declined (Fig. S13b). The decrease of host and viral biodiversity observed for favorable conditions (here, high nutrient) trivially resulted from both communities showing fewer and more similar phenotypes (hosts focused on prioritizing uptake over defense, and viruses focused on exploiting the effectively single host strategy), selected for in high dilution-high nutrient environments.

Interpreting the resulting diversity-nutrient relationship more generically in terms of environmental forcing and costs harmonizes this observation with the apparent contradiction stemming from the classic arguments that link coevolutionary diversification and growth conditions. Environmental forcing that generally decreases the affordability of evolving for all phenotypes deters diversity; however, when that forcing decreases, costs are determined by the dynamic eco-evolutionary interactions of hosts with nutrient and virus, mediated by viral plasticity. The latter are changeable costs that can be compensated differently by phenotypes through various evolutionary strategies, reason why diversity emerges. Thus, the constant biodiversity shown in Fig. 1 would result from these dynamic costs dominating over environmental forcing, whereas high forcing would dominate in correlation with high realized nutrient. In our simulations, high forcing was imposed by high dilution, but the same general conclusion applies to other versions of the model that manipulated the environment in other ways (see SI.8).

Arms races converge to fluctuating selection (Red Queen dynamics) regardless of growth conditions

To understand the underlying coevolutionary dynamics leading to the observations above, and following standard empirical approaches to antagonistic coevolution (e.g.[11]), we also collected in our simulations information about the potential for cross-infection. For all hosts, we checked their immunity to viruses from past, present, and future snapshots; similarly, for all viruses we checked their ability to infect hosts from other snapshots. For early stages of the coevolutionary dynamics (Fig. 3a, b), hosts on average were more immune to past virus phenotypes than future ones, and viruses could infect more past host phenotypes than future ones; this directional evolution is the hallmark of an ongoing arms race[6,11,46]. For later times (Fig. 3c, d), both immunity and range showed oscillatory behavior around constant values, a signature of fluctuating selection or Red-Queen dynamics[6,47]. This shift from one to the other type of evolutionary dynamics has been observed experimentally[16] and has been hypothesized to be driven by evolutionary costs[6,16]. Here, we show that arms races occurred during the transient as host and virus explored the phenotypic space, and the stationary state (with changeable relative abundances for the surviving phenotypes) led to the associated fluctuating selection dynamics (see Fig. S3a–h, and SI.5). Moreover, such a shift occurred regardless of environmental conditions. The transient period, however, was shorter (and therefore the shift occurred earlier) as environmental conditions improved, i.e. for higher dilution or nutrient input.

Past and future empirical work should be considered in light of our observations, to assess whether the duration of experiments captures the evolutionary path and/or the asymptotic evolutionary dynamics. Given our predictions, we re-analyzed existing data from what is, to the best of our knowledge, the only experiment exploring coevolutionary crossinfection for high versus low nutrient input[11]. Differently from earlier conclusions[11,12], the curves obtained with our re-analysis (Fig. 3e–f) would indicate that arms races occurred for both low and high resources. Therefore, longer experiments would have been needed to observe the true, asymptotic evolutionary dynamics of the community. See section SI.5.3 for further details.
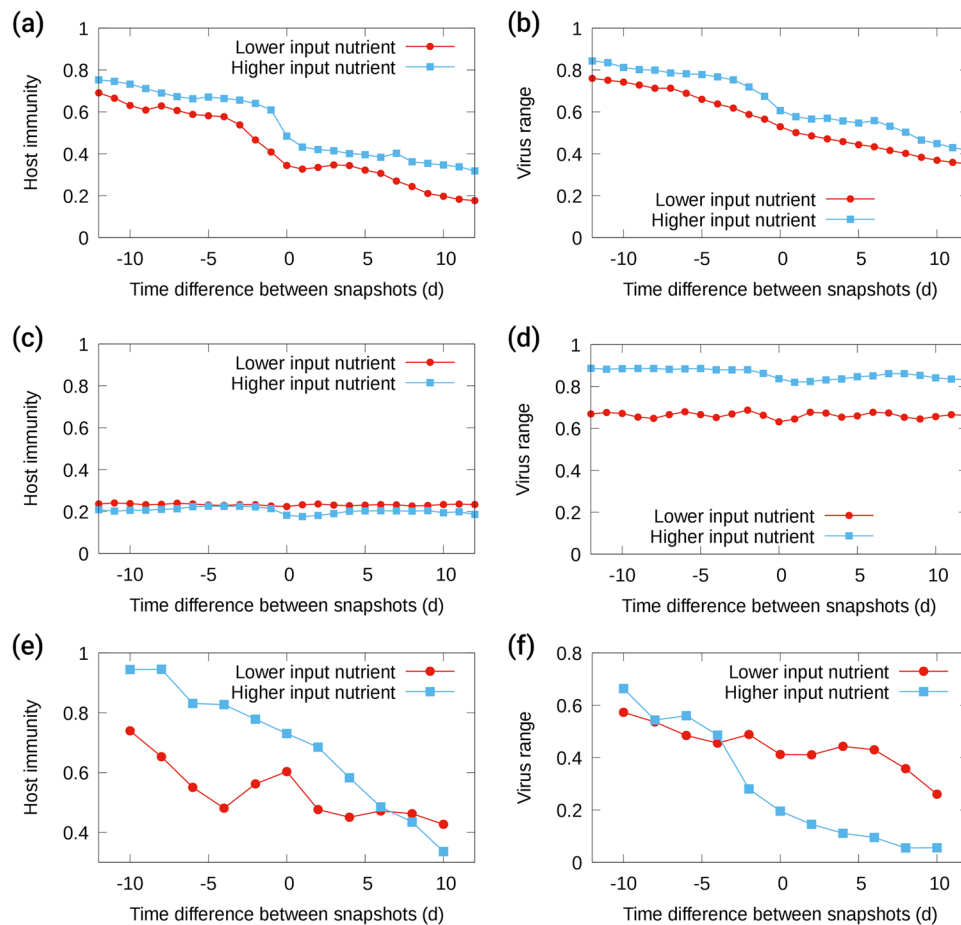
Fig. 3 | Crossinfection results. Top and middle panels (simulations): Data for early stages (first 25 days of the simulation, **a** and **b**) and stationary state (last 25 days of the simulation, **c** and **d**) of the eco-evolutionary dynamics, comparing phenotypes from snapshots taken daily, for a dilution rate $w = 0.2\mu_{max_0} = 6.48 d^{-1}$; circles correspond to our reference input concentration $N_0 = 2.5 \cdot 10^{-5} mol \cdot L^{-1}$, and squares to $N_0 = 10^{-4} mol \cdot L^{-1}$. Arms races drive the early stages of the dynamics (a-b, negative trend), whereas fluctuating selection dynamics occur at the stationary state (c-d, no trend). Oscillatory behavior can be observed for some of the fluctuating selection cases, which points to the presence of demographic oscillations as well. To compare with the empirical data, a time difference up to 12 days is shown using the classic definitions for immunity and range (Eqs. (17–19)); results from simulations using other durations or the biomass-based metrics (Eqs. (18–20)) were qualitatively similar (as long as a stationary state was reached, see SI.5.3). Bottom panels: Curves for host immunity (**e**) and virus range (**f**) obtained averaging the data in refs. 11,12 across replicates; see SI.5.3 for details and Fig. S10 for individual replicates.

Beyond marine ecosystems

Due to their parasitic nature, the performance of any virus should depend to some extent on host physiology and resources. Our results above illustrate that this dependence should be accounted for when studying and predicting the coevolutionary dynamics of any host-virus systems.

For example, phage therapy has been proposed to eliminate antibiotic-resistant bacteria[34,48]; viruses have been engineered to recognize and attach to the receptors of cancer cells and subsequently lyse them[49]; and the potential effects of coevolution on the effectiveness and safety of treatments have been highlighted in the past[50,51]. Our results predict that target cells may diversify under challenging growth conditions, which may lead to undesired consequences (e.g. host cells that are less susceptible to the original phage treatment). Viruses have also been proposed as a way to eliminate bacteria that form biofilms, as the latter reduce the efficacy of conventional treatments[52]. The differential access to resources that bacteria have at e.g. crests and troughs at the irregular biofilm boundaries[53] generates a gradient of growth conditions that, according to our results, would lead to a mosaic of host and virus evolutionary strategies.

The threshold-like behavior observed for immunity and infectivity, unveiled thanks to the measurement of the realized metrics (only accessible through theoretical models) can be used to assess and predict the actual efficacy of phage therapy by mapping, for example, the "classic" observables collected in the laboratory to the realized predictions. Our approach also revealed that the timing of the convergence of arms races to fluctuating selection depends on environmental conditions, information that can be used to assess the duration of a therapy and focus on one or the other regime.

From the virus point of view, the recent SARS-CoV-2 pandemic highlights the need for theories able to predict the rapid evolutionary changes in virus receptor-targeting strategies, which influence the severity of the disease as well as the efficacy of vaccines. Similarly, predicting changes in host range can help anticipate future zoonotic spillover events[54]. Our results show the importance of considering viral plasticity in those predictions.

There are, nonetheless, important assumptions made by the framework that need to be taken into consideration (see SI.9 for a detailed discussion). For example, the framework considers antagonistic coevolution and viral plasticity as main eco-evolutionary drivers; although we show that they are plausible mechanisms underlying the emergent diversity patterns shown in Fig. 1, other ecological and evolutionary aspects could synergistically (or alternatively) participate in these large-scale patterns (see e.g.[31]). Similarly, the parametrization used here focuses on E. coli and T viruses since that is the only system for which viral plasticity functions are available (see Methods);

nonetheless, in our simulations evolution generates rich communities with phenotypes that show a wide variety of defense-counterdefense strategies compatible with those reported for bacteria-phage coevolution generically. In that sense, our results are illustrative of bacteria-virus interactions broadly, although the resulting strategies can be somewhat constrained by the chosen parametrization. An important improvement would introduce a wider initial group explicitly accounting for certain types tailored to the focal example (e.g. SAR11 in the oceans). The addition of other potential sources of top-down regulation (other forms of viral infection such as lysogeny or, in the oceans, grazing by zooplankton), other environmental variables (additional nutrients, temperature), and the replacement of dilution with more realistic environmental forcing specific of the focal example would also improve the framework in important ways[18]. How the patterns above are affected by the inclusion of these elements would help understand their role in such patterns.

Methods

To model the antagonistic coevolution of bacteria and plastic viruses, we modified an eco-evolutionary modeling framework that we successfully used in the past to study host-phage coevolution[55].

Equations for the ecological dynamics

Our model describes the dynamics of uninfected host cells (C, in $cells \cdot L^{-1}$), infected hosts (I, in $cells \cdot L^{-1}$), extracellular viruses (V, in $ind \cdot L^{-1}$), and the concentration of the most limiting nutrient for the host (N, in $mol \cdot L^{-1}$), under controlled environmental conditions (chemostat). The model also explicitly includes the period of infection (latent period, L) by representing the interactions between host cells and viruses through delayed differential equations (see Supplementary Table 1 in SI for symbols and units). For a host phenotype i and a virus phenotype j:

$$\frac{dC_i(t)}{dt} = \mu_i(N)\, C_i - kC_i\left(\sum_m^{n_V} \mathcal{A}_{i,m} V_m\right) - \alpha C_i C_{all} - w C_i \quad (1)$$

$$\frac{dI_i(t)}{dt} = kC_i\left(\sum_m^{n_V} \mathcal{A}_{i,m} V_m\right) - kC_{i,t-L}\left(\sum_m^{n_V} \mathcal{A}_{i,m} V_{m,t-L}\right) e^{-wL} - w I_i \quad (2)$$

$$\frac{dV_j(t)}{dt} = B\,k\left(\sum_m^{n_H} \mathcal{A}_{m,j} C_{m,t-L}\right) V_{j,t-L}\, e^{-wL}$$
$$- k\left(\sum_m^{n_H} \mathcal{A}_{m,j} C_m\right) V_j - \alpha_V V_j V_{all} - d_V V_j - w V_j \quad (3)$$

$$\frac{dN(t)}{dt} = w(N_0 - N) - \frac{1}{Y}\sum_m^{n_H} \mu_m(N) C_m. \quad (4)$$

where n_H and n_V are the total number of host and virus phenotypes at a given time, respectively, and $\mathcal{A}_{i,j} = 1$ if viral phenotype j infects viral host i, or zero otherwise (i.e. $\mathcal{A}$ is the adjacency matrix for the system's interaction network). The first equation (Eq. (1)) represents, for a given host phenotype, the dynamics of the population of uninfected cells, which increases at a growth rate μ that depends on the availability of the most limiting nutrient (first term), and declines due to adsorption and infection by any extracellular viruses able to infect this host (second term) or dilution from the chemostat at a rate w (fourth term). The third term accounts for potential competition among all host phenotype populations for space or resources not explicitly modeled that can affect negatively the growth of the focal phenotype, especially relevant as the eco-evolutionary framework allows for many contemporary host phenotype populations; $C_{all} = \sum_i C_i$ thus represents

uninfected cells across all phenotypes (see SI.9.2). As usually assumed in host-virus models, all adsorptions lead to infection (first term in Eq. (2)); in addition, the population of infected cells declines due to dilution (third term) or due to lysis (second term), with the number of lysed cells calculated as the cells that were infected a latent period in the past (i.e. at time $t − L$) and avoided dilution during that latent period (which occurs at a probability given by e^{-wL}). Each lysed cell produces B new extracellular viruses (first term in Eq. (3)), whose population decreases as they enter/infect uninfected cells (second term), decay and lose infectivity (fourth term), or are diluted (fifth term). The third term represents superinfection avoidance, generically accounting for the battery of mechanisms that an infecting virus can deploy to prevent any other virus from using the same host for replication[8]; to this end, we used a density-dependent term where $V_{all} = \sum_j V_j$ represents the sum of all (extracellular) virus densities across phenotypes (see SI.9.2). Finally, Eq. (4) represents the dynamics of the most limiting nutrient for the host population, whose availability changes due to inflow and dilution from the chemostat (first term), and decreases as it is taken up by uninfected hosts within the chemostat (second term). Also a typical assumption, infected cells do not grow nor replicate, and thus they do not contribute to the uptake term nor need to be considered for the third term in Eq. (1). Nutrient uptake results from the host's requirement for growth, provided by the classic Monod formulation[56]:

$$\mu = \mu_{max}\frac{N}{N + K_N}, \quad (5)$$

where μ_{max} is the maximum growth rate (in d^{-1}), and K_N is the half-saturation constant for growth on the focal nutrient (in $mol \cdot L^{-1}$).

As commonly done in population models, we set a threshold below which either the host or the viral populations were considered to be extinct, which avoids unrealistically low values of either population as well as potential population "regeneration" from such unrealistic values. Here, we set a threshold of 1 $ind \cdot L^{-1}$ for either population; in the case of the virus, the threshold applied to both extracellular and intracellular viruses together, a conservative choice aimed to prevent eliminating newly introduced viral mutant populations while still within infected cells before completing their first lytic cycle.

Although the equations above can represent the ecological dynamics of a wide variety of host-virus systems, here we focused on *Escherichia coli* as a host and T7 phage as the virus. The wealth of information available about this system enabled the parametrization of the equations above, including expressions for the dependence of the viral traits on host physiology (viral plasticity, see below). The focal nutrient was glucose, which E. coli uses to sustain growth, but other nutrient choices more relevant for other organisms or environments (e.g. nitrogen) can be used by modifying the nutrient-related parameters (see Supplementary Table 1 in SI). Additionally, although the equations above can be easily adapted to other settings, chemostats are highly tunable by modifying the dilution rate, w, or the input concentration, N_0, which we used here to achieve a gradient of growth conditions. Moreover, chemostats can represent a variety of environments, from volumes of water in the ocean (with inflow/outflow representing advection that moves nutrients, hosts, and viruses in/out of the focal volume, and turbulence mixing the medium), to different areas of the human intestinal tract (with inflow/outflow representing directional tract flows).

Host traits and tradeoffs

Here, we focused on one single type of host receptor as viral gateway for infection; we considered that evolution can alter the physical configuration of such receptor, which can prevent infection by viruses unable to recognize and attach to this evolved form (Fig. 1a). From the

wide variety of defense mechanisms that hosts can develop, such an evolutionary response is one of the quickest and most well-documented defense strategies for microbes[7,14,34].

Each host phenotype was therefore characterized by a fixed number of specific, identical receptors (i.e. each phenotype showed only one receptor type), which in turn were defined by how much they departed from the pristine form of the receptor. We used a real value $a \in [a_{min}, a_{max}]$ to represent quantitatively the form of the receptor, with $a = a_0$ representing the pristine form. Thus, a was the only host evolving trait, and host phenotypes differed in the value of a (and related traits, see Eq. (7) below) and were identical otherwise. For the results presented here, $a \in [0, 2]$ and $a_0 = 1$, but other values did not change qualitatively our results (as long as the values of a_{min} and a_{max} do not cap/constrain evolution, a standard caution in any model that accounts for evolutionary dynamics).

The evolution of the receptor typically leads to a decrease in its nutrient-uptake efficiency, which ultimately translates into a decrease in the overall host growth rate[6,7,14,36]. Here, we represented such a tradeoff with a reduction of the maximum growth rate (which links growth and nutrient uptake, Eq. (5)) proportional to how much the receptor departed from its pristine form (i.e. degree of innovation). In short, μ_{max} decreased linearly as the receptor characterizing the phenotype departed from the pristine form; phenotypes with the pristine receptor showed full growth potential (i.e. $\mu_{max} = \mu_{max_0}$), whereas that potential was reduced to $\mu_{max} = \epsilon_\mu \mu_{max_0}$ for those phenotypes whose receptors showed the highest possible degree of innovation (Fig. S1b). Here, we set ϵ_μ to a low but non-zero value, $\epsilon_\mu = 0.05$, representing the fact that even the most evolved receptor can still be somewhat functional. Mathematically, we defined the degree of innovation for a given host phenotype i as:

$$\Delta_i = \left| \frac{a_i - a_0}{a_0} \right|, \tag{6}$$

confined between a minimum and a maximum distance to the pristine receptor, $[\Delta_{min} = 0, \Delta_{max} = max(\Delta(a_{max}), \Delta(a_{min}))]$ (see Fig. S1a). Thus, the phenotype's maximum growth rate was given by:

$$\mu_{max_i} = \mu_{max_0} (1 - c_a \Delta_i) \tag{7}$$

where c_a is a constant to map the parenthesis into $[\epsilon_\mu, 1]$:

$$c_a = \frac{1 - \epsilon_\mu}{\Delta_{max}} \tag{8}$$

Note that the second term in the parenthesis, $c_a \Delta_i$, effectively quantifies the cost of innovation (i.e. distance between the realized μ_{max} and pristine performance μ_{max_0}).

In our simulations, no surviving phenotype reached the proximity of the interval limits for a, and thus never showed maximal innovation ($\Delta = 1$ with the chosen parametrization). On the other hand, receptor evolution did not affect the other host traits in the model (the Monod-related half saturation constant, K_N, and yield, Y).

Viral traits and tradeoffs

As a viral evolutionary response, we focused on increases in the versatility of the viral tail fiber to recognize and attach to diverse forms of the focal receptor (Fig. 1a), a viral counter-defense response that has been shown to emerge shortly after hosts evolve modifications to their receptors[6,14,33].

Viral phenotypes were here characterized by the set of receptor forms that they could recognize. Thus, we assigned to each phenotype an array $\mathbf{r}$ of $R = 10$ possible integers between 1 and R, with each integer representing forms of the receptor (i.e. values of a) that the virus could recognize. Specifically, a viral phenotype j was able to target a host

phenotype i if $d_i \in \mathbf{r}_j$, where d_i is the integer resulting from mapping a_i into $1, \ldots, R$:

$$d_i = c_{1,r} a_i + c_{2,r} \tag{9}$$

and:

$$c_{1,r} = \frac{R - 1}{a_{max} - a_{min}}, \quad c_{2,r} = \frac{a_{max} - a_{min}R}{a_{max} - a_{min}} \tag{10}$$

Therefore, with the parametrization chosen here (see Supplementary Table 1 in SI), a viral phenotype with a value $r_0 = 5$ within its $\mathbf{r}$ array would be able to target hosts whose a is within [0.889, 1.111], which encompasses not only the pristine form of the receptor $a_0 = 1$ but also slightly modified versions of it (Fig. S2). The latter, necessary from a technical standpoint because a is represented using real numbers, reflects the fact that only after evolution has modified a receptor sufficiently does the tail fiber lose the ability to recognize and attach to it. Virus phenotypes thus differed only if the list of distinct integers within their $\mathbf{r}$ array differed (see Fig. S2). The versatility of phenotype j was defined as the number of distinct integers within $\mathbf{r}_j$, n_{diff_j}.

Following empirical evidence, we also considered the observed decrease in infection efficiency shown by viruses that evolve a higher versatility[6,14,33,35], here represented as a decrease in the adsorption rate proportional to n_{diff}. In short, viruses with only one distinct integer in the array (i.e. targeting a single type of receptor) showed the maximum possible adsorption rate, k_0, whereas the most versatile viruses (i.e. R distinct integers in the $\mathbf{r}$ array) showed a reduced adsorption rate $\epsilon_k k_0$ (Fig. S1c). Here, we set $\epsilon_k = 0.1$, which aimed to represent a non-zero minimum adsorption efficiency even for the most versatile phenotypes. Mathematically:

$$k_j = k_0 \left[1 - c_{1,k} \left(n_{diff_j} - 1 \right) \right], \tag{11}$$

where $c_{1,k}$ helps map the bracket above into the interval $[\epsilon_k, 1]$:

$$c_{1,k} = \frac{1 - \epsilon_k}{R - 1} \tag{12}$$

Note that the second term in the bracket, $c_{1,k}(n_{diff_j} - 1)$, effectively quantifies the cost of versatility (i.e. distance between the realized k and k_0).

In our simulations, no surviving viral phenotype reached full versatility ($n_{diff} = R$, see below). We assumed that tail fiber evolution did not affect the other viral traits considered in the model. Such traits are defined by the lytic cycle[57]: after attaching to the host receptor and injecting their genetic material into the host, viruses hijack the host machinery and use host resources to i) synthesize the components of the new virions during the eclipse period E, and ii) assemble those components at a certain maturation rate M to form the new mature individuals released at lysis; the total infection time (from adsorption to lysis) is the latent period L, and the number of new virions released per infection is the burst size B.

Modeling viral plasticity. As described above for the lytic cycle, due to its parasitic nature the virus utilizes the host synthesis machinery and resources to replicate. This leads to an obvious link between host physiological state and viral reproduction that has been identified experimentally in a multitude of systems[19,23,26–30], but so far only systematically studied for the E. coli - T virus system[20,22,24,25].

Such a link has been characterized as a relationship between viral traits and host growth rate, termed viral plasticity because the value of viral traits changes as the host (reproductive environment of the virus) changes. In the past, we compiled existing data for E. coli and T phage and found that the eclipse period, E, and maturation rate, M, could be

expressed as the following functions[40]:

$$E(\mu) = E_\infty + E_0 e^{-\alpha_E \mu / \mu_{max_0}} \tag{13}$$

$$M(\mu) = \frac{M_\infty}{1 + e^{-\alpha_M (\mu / \mu_{max_0} - M_0)}} \tag{14}$$

where μ represents the host growth rate at the moment of infection, with the implicit assumption that it remains constant during the latent period[20,22]. In short, these functions illustrate that, as the host growth rate gets closer to its maximum potential value, μ_{max_0}, the time needed to synthesize virion components decreases and the rate to assemble them into mature viruses increases. Both traits reach a lower and upper plateau, respectively, due to physiological constraints and bottlenecks. See[40] and references therein for more details. We also showed that the optimal latent period under chemostat conditions can be written as[40]:

$$L(\mu) = L_0 + E(\mu), \tag{15}$$

where $L_0 = 1/w$, and thus is set by the chemostat dilution rate; in other words, this optimal latent period has an environmental component L_0 and a component provided by the (plastic) eclipse period. Here, we assumed this optimal latent period for all viruses as a way to consider the most dominant L value expected for a given chemostat, and thus to focus solely on the evolution of versatility (Fig. S1d). See SI.9.4 for a discussion on other choices for L_0. Regarding the burst size, we used a modified version of an empirically derived expression[58]:

$$B(\mu) = M(\mu)[L(\mu) - E(\mu)], \tag{16}$$

where we only added the potential for the traits involved to depend on host physiology, ultimately leading to a dependence of burst size on host growth rate (see Fig. S1e).

Eqs. (13–16) thus link the trait values for a given viral individual to the growth rate (at time of infection) of the individual host cell it infects.

Nonplastic version of the model. To understand the role of viral plasticity in antagonistic coevolution, we contrasted the results obtained using the expressions above (Eqs. (13–16)) with those obtained with a version of the model that uses fixed values for those viral traits. The latter can represent both an example of a virus that depends minimally on the host (taken to the extreme of no dependence at all) as well as the expectations built with standard models, which neglect viral plasticity.

To obtain fixed values for the latent period and burst size that still represented the most dominant viral trait values expected at a given environment, we used Eqs. (15) and (16) with a fixed value for the eclipse period and the maturation rate, E_{non} and M_{non} respectively. For these two traits, the typical information available is from laboratory experiments in which, as explained in ref. 20, the host is kept under maximal growth conditions. Thus, for coherence we calculated those values here by using Eqs. (13) and (14) with $\mu = \mu_{max_0}$ (i.e. $E_{non} = E(\mu_{max_0}), M_{non} = M(\mu_{max_0})$), which were within the ranges reported in the literature for T viruses (e.g.[20,22,59]). Therefore, the resulting $L_{non} = L(\mu_{max_0})$ and $B_{non} = B(\mu_{max_0})$ provided values for the most dominant L and B that are expected for a given environment, but that disregard plasticity.

Modeling evolution
To model the evolution of the focal traits (host receptor and viral tail fiber), we adapted an eco-evolutionary approach that has been repeatedly used in the literature for a variety of microbial systems and questions (e.g.[40,42,47,55,60]).

Generically, for one evolving species the approach considers mutation events occurring at exponentially distributed times that depend on the species' mutation rate. At each mutation time, ecological dynamics are stopped to use a roulette-wheel genetic algorithm that determines which phenotype evolves, chosen with a probability that depends on each phenotype's relative abundance. A new mutant population is introduced then in the system, in small numbers, that is identical to the parental phenotype except for a small, random difference in the evolving trait. Thus, ecological dynamics resume and the new and existing phenotypes interact (e.g. compete), with some of such populations consequently growing in numbers and others going extinct, until a new mutation event occurs. This "innovation+selection" iterative process allows the system to explore the trait space, with the possibility of reaching an evolutionarily stable strategy (ESS, trait fixation or selective sweeping), or the continued coexistence of several dominating phenotypes with or without evolutionary oscillations (fluctuating selection or Red Queen dynamics). Because mutation times are randomly selected based on the demography of the evolving population, there is no imposed separation of ecological and evolutionary timescales, and thus the emerging evolutionary dynamics are affected by the ecological interactions and vice-versa (eco-evolutionary dynamics).

In our case, both host and virus evolved. At any given time, existing host and virus phenotype populations interacted following Eqs. (1–16), with hosts competing for the available nutrients and viruses competing for common hosts. These ecological interactions were simulated using a tailored Euler scheme to integrate the system of delayed differential equations, but any other solver accounting for the delay (i.e. latent-period-related) terms can be used. Mutation times for the host were determined by the host mutation rate (see Supplementary Table 1 in SI) and the population densities of the existing host phenotypes, the latter also influencing each phenotype's mutation probability (i.e. probability to be chosen for mutation). New host mutants introduced in the system were identical to the parental phenotype except for the value of a, which differed by an amount randomly distributed in $\mathcal{N}(0, \sigma_a)$ (i.e. Gaussian distribution with mean 0 and standard deviation σ_a). We considered two phenotypes to be identical if their a differed less than $da = 10^{-2}$. On the other hand, mutation times for the virus were determined by the viral mutation rate (see Supplementary Table 1 in SI) and the population densities of the existing viral phenotypes, which also determined their respective mutation probability. Through mutations in the tail fiber, mutant viral phenotypes showed the same **r** array as the parental phenotype except for a randomly chosen location, where a new integer was considered that resulted from adding a random amount (from a standard normal distribution, $\mathcal{N}(0,1)$) to the existing integer, then converting the result back to an integer. This rule ensured that any new form of the receptor that can be recognized as a result of the mutation was not radically different from the ones the parental phenotype could attach to, in agreement with empirical observations that evolution of a wider range results from cumulative evolutionary steps[61]. We considered two phenotypes to be identical if their **r** showed the same set of distinct (i.e. non-repeated) integers, which would mean that they targeted the same receptors (i.e. showed the same strategy). After a new mutant phenotype was introduced, the ecological dynamics resumed. Mutation times were stochastic and did not necessarily occur after ecology reached an equilibrium, thus enabling eco-evolutionary interactions.

We started our simulations with one single phenotype population with the pristine form of the receptor, i.e. characterized by $a = a_0$, and one single viral phenotype with all locations in **r** set to $r_0 = 5$, i.e. able to infect only the pristine form of the receptor.

Due to the random nature of the evolutionary algorithm, we used 100 replicates for each of the cases explored here. We stopped each replicate after $t = 10^5 d$ to ensure that the system had reached its asymptotic eco-evolutionary behavior regardless of the environmental conditions (the latter set by the dilution rate, w, and nutrient input

concentration, N_0). See Supplementary Table 1 in SI for more information regarding the chosen parametrization.

Measures of strategy effectiveness and diversity

To measure the effectiveness of a given host strategy, we used the standard measure of resistance or immunity, i.e. proportion of virus phenotypes that a given host phenotype i can elude[16]:

$$\nu_i = 1 - \frac{\sum_j \mathcal{A}_{i,j}}{n_V}, \tag{17}$$

where n_V is the total number of virus phenotypes at a given time and, as above, $\mathcal{A}_{i,j} = 1$ if viral phenotype j infects viral host i, or zero otherwise. Because we can monitor the abundance of all host and viral phenotype populations, we also measured a weighted version of such immunity:

$$\nu_{w_i} = 1 - \frac{\sum_j \mathcal{A}_{i,j} V_j}{V_{all}}. \tag{18}$$

This expression accounts for the proportion of the total virus abundance that cannot infect the focal virus phenotype, and therefore reflects more closely the success of a host strategy: large values indicate the ability of the host phenotype to elude the majority of available extracellular viruses, regardless of whether they belong to one or many different phenotypes. We will refer to ν_w as realized immunity hereon.

To measure the effectiveness of a given viral strategy, we used the standard measure of range, i.e. proportion of host phenotypes that a given virus phenotype j can infect[16]:

$$\rho_j = \frac{\sum_i \mathcal{A}_{i,j}}{n_H}, \tag{19}$$

where n_H is the total number of host phenotypes at a given time. As in the case of immunity, we also measured a weighted version:

$$\rho_{w_j} = \frac{\sum_i \mathcal{A}_{i,j} C_i}{C_{all}}, \tag{20}$$

which accounts for the proportion of the total host biomass that is infected by the focal virus phenotype. This expression thus reflects more closely the success of a viral strategy: large values indicate the ability of the virus phenotype to infect the majority of available host cells, regardless of whether they belong to one or many different phenotypes. We will refer to ρ_w as realized infectivity hereon.

Finally, we used the standard definition of richness as the number of phenotypes (n_H for host, n_V for virus), and the Shannon index[44] as a measure of biodiversity, defined as:

$$S_H = - \sum_i \left(\frac{C_i}{C_{all}} \right) \log \left(\frac{C_i}{C_{all}} \right) \tag{21}$$

for the host and:

$$S_V = - \sum_j \left(\frac{V_j}{V_{all}} \right) \log \left(\frac{V_j}{V_{all}} \right) \tag{22}$$

for the virus.

Reporting summary

Further information on research design is available in the Nature Portfolio Reporting Summary linked to this article.

Data availability

No new empirical data were generated for this study. Information regarding how the empirical data re-analyzed here were originally collected and how to download them can be found in the corresponding publications[11,12,31,32]. The Tara Oceans data used here (Figs. 1b–d, S15) are available in refs. 62–65, but note that the consortium may make available updated versions of the data. The empirical crossinfection data analyzed for Fig. 3e–f are available in ref. 12. All simulation data regarding Figs. 1e–f, 2, 3a–d, or any of the simulation Supplementary Figs. can be generated and analyzed with the code provided, but specific subsets can be made available upon request. See also Code availability statement and Reporting Summary.

Code availability

The code developed to run the simulations and all analyses, including analysis of empirical data, is available at https://doi.org/10.17605/OSF.IO/YS9AW.

References

1. Fuhrman, J. A. Marine viruses and their biogeochemical and ecological effects. *Nature* **399**, 541–548 (1999).
2. Suttle, C. A. Marine viruses — major players in the global ecosystem. *Nat. Rev. Microbiol.* **5**, 801–812 (2007).
3. Breitbart, M. Marine viruses: Truth or dare. *Ann. Rev. Mar. Sci.* **4**, 425–448 (2012).
4. Roux, S. et al. Ecogenomics and potential biogeochemical impacts of globally abundant ocean viruses. *Nature* **537**, 689–693 (2016).
5. Locke, H. et al. Chapter two - marine viruses and climate change: Virioplankton, the carbon cycle, and our future ocean. In Roossinck, M. J. (ed.) *Viruses and Climate Change*, vol. 114 of *Advances in Virus Research*, 67–146 (Academic Press, 2022).
6. Martiny, J. B., Riemann, L., Marston, M. F. & Middelboe, M. Antagonistic coevolution of marine planktonic viruses and their hosts. *Annu. Rev. Mar. Sci.* **6**, 393–414 (2014).
7. Dy, R. L., Richter, C., Salmond, G. P. C. & Fineran, P. C. Remarkable mechanisms in microbes to resist phage infections. *Annu. Rev. Virol.* **1**, 307–331 (2014).
8. van Houte, S., Buckling, A. & Westra, E. R. Evolutionary ecology of prokaryotic immune mechanisms. *Microbiol. Mol. Biol. Rev.* **80**, 745–763 (2016).
9. Koskella, B. & Brockhurst, M. A. Bacteria–phage coevolution as a driver of ecological and evolutionary processes in microbial communities. *FEMS Microbiol Rev. 3* **38**, 916–931 (2014).
10. Lopez Pascua, L. & Buckling, A. Increasing productivity accelerates host–parasite coevolution. *J. Evol. Biol.* **21**, 853–860 (2008).
11. Lopez Pascua, L. et al. Higher resources decrease fluctuating selection during host–parasite coevolution. *Ecol. Lett.* **17**, 1380–1388 (2014).
12. Fortuna, M. A. et al. Coevolutionary dynamics shape the structure of bacteria-phage infection networks. *Evolution* **74**, 1001–1011 (2019).
13. Forde, S. E., Thompson, J. N., Holt, R. D. & Bohannan, B. J. M. Coevolution drives temporal changes in fitness and diversity across environments in a bacteria-bacteriophage interaction. *Evolution* **62**, 1830–1839 (2008).
14. Bohannan, B. J. M. & Lenski, R. E. Linking genetic change to community evolution: insights from studies of bacteria and bacteriophage. *Ecol. Lett.* **3**, 362–377 (2000).
15. Middelboe, M., Holmfeldt, K., Riemann, L., Nybroe, O. & Haaber, J. Bacteriophages drive strain diversification in a marine flavobacterium: implications for phage resistance and physiological properties. *Environ. Microbiol.* **11**, 1971–1982 (2009).
16. Hall, A. R., Scanlan, P. D., Morgan, A. D. & Buckling, A. Host–parasite coevolutionary arms races give way to fluctuating selection. *Ecol. Lett.* **14**, 635–642 (2011).

17. Marston, M. F. et al. Rapid diversification of coevolving marine synechococcus and a virus. *Proc. Natl Acad. Sci. USA* **109**, 4544–4549 (2012).

18. Zimmerman, A. et al. Metabolic and biogeochemical consequences of viral infection in aquatic ecosystems. *Nat. Rev. Microbiol.* **18**, 21–34 (2020).

19. Webb, V., Leduc, E. & Spiegelman, G. B. Burst size of bacteriophage sp82 as a function of growth rate of its host bacillus subtilis. *Can. J. Microbiol.* **28**, 1277–1280 (1982).

20. Hadas, H., Einav, M., Fishov, I. & Zaritsky, A. Bacteriophage T4 development depends on the physiology of its host Escherichia coli. *Microbiol.* **143**, 179–185 (1997).

21. Middelboe, M. Bacterial growth rate and marine virus-host dynamics. *Microb. Ecol.* **40**, 114–124 (2000).

22. You, L., Suthers, P. F. & Yin, J. Effects of Escherichia coli physiology on growth of phage T7 in vivo and in silico. *J. Bacteriol.* **184**, 1888–1894 (2002).

23. Gnezda-Meijer, K., Mahne, I., Poljsak-Prijatelj, M. & Stopar, D. Host physiological status determines phage-like particle distribution in the lysate. *FEMS Microbiol. Ecol.* **55**, 136–145 (2006).

24. Birch, E. W., Ruggero, N. A. & Covert, M. W. Determining host metabolic limitations on viral replication via integrated modeling and experimental perturbation. *PLoS Comput. Biol.* **8**, e1002746 (2012).

25. Golec, P., Karczewska-Golec, J., Los, M. & Wegrzyn, G. Bacteriophage T4 can produce progeny virions in extremely slow growing Escherichia coli host: comparison of a mathematical model with the experimental data. *FEMS Microbiol. Lett.* **351**, 156–161 (2014).

26. Bratbak, G., Jacobsen, A., Heldal, M., Nagasaki, K. & Thingstad, F. Virus production in phaeocystis pouchetii and its relation to host cell growth and nutrition. *Aquat. Microb. Ecol.* **16**, 1–9 (1998).

27. Piedade, G., Wesdorp, E., Montenegro-Borbolla, E., Maat, D. & Brussaard, C. Influence of irradiance and temperature on the virus mpov-45t infecting the arctic picophytoplankter micromonas polaris. *Viruses* **10**, 676 (2018).

28. Cheng, K., Frenken, T., Brussaard, C. & Van de Waal, D. Cyanophage propagation in the freshwater cyanobacterium phormidium is constrained by phosphorus limitation and enhanced by elevated pco2. *Front. Microbiol.* **10**, 617 (2019).

29. Kranzler, C. et al. Silicon limitation facilitates virus infection and mortality of marine diatoms. *Nat. Microbiol.* **4**, 1790–1797 (2019).

30. Kranzler, C. et al. Impaired viral infection and reduced mortality of diatoms in iron-limited oceanic regions. *Nat. Geosci.* **14**, 231–237 (2021).

31. Ibarbalz, F. M. et al. Global trends in marine plankton diversity across kingdoms of life. *Cell* **179**, 1084–1097.e21 (2019).

32. Dominguez-Huerta, G. et al. Diversity and ecological footprint of global ocean rna viruses. *Science* **376**, 1202–1208 (2022).

33. Scanlan, P., Hall, A., Lopez-Pascua, L. & Buckling, A. Genetic basis of infectivity evolution in a bacteriophage. *Mol. Ecol.* **20**, 981–989 (2011).

34. Mizoguchi, K. et al. Coevolution of bacteriophage pp01 and escherichia coli o157:h7 in continuous culture. *Appl. Environ. Microbiol.* **69**, 170–176 (2003).

35. Bohannan, B. J. M., Kerr, B., Jessup, C. M., Hughes, J. B. & Sandvik, G. Trade-offs and coexistence in microbial microcosms. *Antonie van. Leeuwenhoek* **81**, 107–115 (2002).

36. Lennon, J., Khatana, S., Marston, M. & Martiny, J. B. H. Is there a cost of virus resistance in marine cyanobacteria? *ISME J.* **1**, 300–312 (2007).

37. Poullain, V., Gandon, S., Brockhurst, M. A., Buckling, A. & Hochberg, M. E. The evolution of specificity in evolving and coevolving antagonistic interactions between a bacteria and its phage. *Evolution* **62**, 1–11 (2008).

38. Duffy, S., Turner, P. E. & Burch, C. L. Pleiotropic costs of niche expansion in the rna bacteriophage φ6. *Genetics* **172**, 751–757 (2006).

39. Avrani, S., Wurtzel, O., Sharon, I., Sorek, R. & Lindell, D. Genomic island variability facilitates prochlorococcus–virus coexistence. *Nature* **474**, 604–608 (2011).

40. Choua, M. & Bonachela, J. A. Ecological and evolutionary consequences of viral plasticity. *Am. Nat.* **193**, 346–358 (2019).

41. Heineman, R. H. & Bull, J. J. Testing optimality with experimental evolution: lysis time in bacteriophage. *Evolution* **61**, 1695–1709 (2007).

42. Bonachela, J. A. & Levin, S. A. Evolutionary comparison between viral lysis rate and latent period. *J. Theor. Biol.* **345**, 32–42 (2014).

43. Winter, C., Bouvier, T., Weinbauer, M. G. & Thingstad, T. F. Trade-offs between competition and defense specialists among unicellular planktonic organisms: the "killing the winner" hypothesis revisited. *Microbiol. Mol. Biol. Rev.* **74**, 42–57 (2010).

44. Shannon, C. E. A mathematical theory of communication. *Bell Syst. Techl.* **27**, 623–656 (1948).

45. Raes, E. J., Bodrossy, L., van de Kamp, J., Bissett, A. & Waite, A. M. Marine bacterial richness increases towards higher latitudes in the eastern indian ocean. *Limnol. Oceanogr. Lett.* **3**, 10–19 (2018).

46. Weitz, J. S., Hartman, H. & Levin, S. A. Coevolutionary arms races between bacteria and bacteriophage. *Proc. Natl Acad. Sci. USA* **102**, 9535–9540 (2005).

47. Bonachela, J. A., Wortel, M. & Stenseth, N. C. Eco-evolutionary red queen dynamics regulate biodiversity in a metabolite-driven microbial system. *Sci. Rep.* **7**, 17655– (2017).

48. Weld, R. J., Butts, C. & Heinemann, J. A. Models of phage growth and their applicability to phage therapy. *J. Theor. Biol.* **227**, 1–11 (2004).

49. Dart, A. Phage warriors. *Nat. Rev. Cancer* **19**, 544–545 (2019).

50. Brockhurst, M. A., Koskella, B. & Zhang, Q.-G. Bacteria-phage antagonistic coevolution and the implications for phage therapy. In Harper, D., Abedon, S., Burrowes, B. & McConville, M. (eds.) *Bacteriophages: Biology, Technology, Therapy*, 1–21 (Springer International Publishing, Cham, 2017).

51. Monferrer, E. & Domingo-Calap, P. Virus-host coevolution as a tool for controlling bacterial resistance to phage therapy. *J. Biotechnol. Biomed.* **2**, 96–104 (2019).

52. Ferriol-Gonzĺez, C. & Domingo-Calap, P. Phages for biofilm removal. *Antibiotics* **9**, 268 (2020).

53. Bonachela, J. A., Nadell, C. D., Xavier, J. B. & Levin, S. A. Universality in bacterial colonies. *J. Stat. Phys.* **144**, 303–315 (2011).

54. Ellwanger, J. H. & Bogo Chies, J. A. Zoonotic spillover: Understanding basic aspects for better prevention. *Genet. Mol. Biol.* **44**, e20200355 (2021).

55. Bonachela, J. A., Choua, M. & Heath, M. R. Unconstrained coevolution of bacterial size and the latent period of plastic phage. *PLoS ONE* **17**, e0268596 (2022).

56. Monod, J. Technique de culture continue. theory et applications. *Ann. Inst. Pasteur* **79**, 390–410 (1950).

57. Weinbauer, M. G. Ecology of prokaryotic viruses. *FEMS Microbiol. Rev.* **28**, 127–181 (2004).

58. Wang, I.-N. Lysis timing and bacteriophage fitness. *Genetics* **172**, 17–26 (2006).

59. Abedon, S. T., Herschler, T. & Stopar, D. Bacteriophage latent-period evolution as a response to resource availability. *Appl. Environ. Microbiol.* **67**, 4233–4241 (2001).

60. Menge, D. N. L. & Weitz, J. S. Dangerous nutrients: evolution of phytoplankton resource uptake subject to virus attack. *J. Theor. Biol.* **257**, 104–115 (2009).

61. Hall, A. R., Scanlan, P. D. & Buckling, A. Bacteria-phage coevolution and the emergence of generalist pathogens. *Am. Nat.* **177**, 44–53 (2011).

62. Ibarbalz, F. M. Tara oceans - marine plankton diversity, mendeley data, v2.
63. Ibarbalz, F. M. Tara oceans consortium, coordinators; tara oceans expedition, participants (2017): Registry of all samples from the tara oceans expedition pangaea. (2009-2013).
64. Salazar, G. Supplementary information for samples and data used in salazar et al. gene expression changes and community turnover differentially shape the global ocean metatranscriptome. (2019).
65. Dominguez-Huerta, G. et al. Diversity and ecological footprint of global ocean rna viruses. data sets. https://bitbucket.org/MAVERICLab/global-rna-virus-ecology-2022/src/master/Fig3/.

Acknowledgements

Author contributions

Model development, simulations, and all analyses performed by J.A.B., as well as manuscript writing and editing.

Competing interests

The author declares no competing interests.

Additional information

Supplementary information The online version contains supplementary material available at https://doi.org/10.1038/s41467-024-51344-3.

Correspondence and requests for materials should be addressed to Juan A. Bonachela.

Peer review information *Nature Communications* thanks Amy Zimmerman, and the other, anonymous, reviewers for their contribution to the peer review of this work. A peer review file is available.

Reprints and permissions information is available at http://www.nature.com/reprints

Publisher's note Springer Nature remains neutral with regard to jurisdictional claims in published maps and institutional affiliations.